Numerical Heat Transfer, Part A, 45: 751–776, 2004

ISSN: 1040-7782 print/1521-0634 online
DOI: 10.1080/10407780490424280

Taylor & Francis
Taylor & Francis Group

A COMPUTATIONAL MODEL OF COUPLED HEAT AND MOISTURE TRANSFER WITH PHASE CHANGE IN GRANULAR SUGAR DURING VARYING ENVIRONMENTAL CONDITIONS

Junye Wang, Nicholas Christakis, Mayur K. Patel, and Mark Cross
Centre for Numerical Modelling and Process Analysis, School of Computing and Mathematical Sciences, The University of Greenwich, London, UK

Mark C. Leaper
Formerly The Wolfson Centre for Bulk Solids Handling Technology, The University of Greenwich, London, UK

As part of a comprehensive effort to predict the development of caking in granular materials, a mathematical model is introduced to model simultaneous heat and moisture transfer with phase change in porous media when undergoing temperature oscillations/cycling. The resulting model partial differential equations were solved using finite-volume procedures in the context of the PHYSICA framework and then applied to the analysis of sugar in storage. The influence of temperature on absorption/desorption and diffusion coefficients is coupled into the transport equations. The temperature profile, the depth of penetration of the temperature oscillation into the bulk solid, and the solids moisture content distribution were first calculated, and these proved to be in good agreement with experimental data. Then, the influence of temperature oscillation on absolute humidity, moisture concentration, and moisture migration for different parameters and boundary conditions was examined. As expected, the results show that moisture near boundary regions responds faster than farther away from them with surface temperature changes. The moisture absorption and desorption in materials occurs mainly near boundary regions (where interactions with the environment are more pronounced). Small amounts of solids moisture content, driven by both temperature and vapour concentration gradients, migrate between boundary and center with oscillating temperature.

Received 21 February 2003; accepted 13 October 2003.

This work forms part of the coordinated research project in Quality in Particulate Manufacturing (QPM) funded by EPSRC Innovative Manufacturing Initiative for Process Industries (grant reference: GR/M15057/01), whose support is gratefully acknowledged.

Address correspondence to Mayur K. Patel, Centre for Numerical Modelling and Process Analysis, School of Computing and Mathematical Sciences, The University of Greenwich, London SE18 6PF, UK. E-mail: M.K.Patel@gre.ac.uk

NOMENCLATURE

A	surface area of a single particle, m^2	T_m	oscillating temperature average, °C
b	radius at the narrowest part of the liquid bridge, m	T_s	temperature of exposed surface, °C
		V	volume of a single particle, m^3
c_{ps}	specific heat of granulated sugar, J/kg°C	W	moisture content of granulated sugar, % of kg water/kg sugar
C_1, C_2	constants in Eq. (11)	W_0	initial moisture content of granulated sugar, % of kg water/kg sugar
D_a	diffusion coefficient of water vapor in air, m^2/s	W_{eq}	equilibrium moisture content of granulated sugar, % of kg water/kg sugar
D_e	effective diffusion coefficient of water vapor, m^2/s		
ERH	equilibrium relative humidity of air	Y	absolute humidity of air, kg water/kg dry air
F	sum of areas of all particles in unit volume, m^2	Y_0	initial absolute humidity of air, kg water/kg dry air
k	mass transfer coefficient for sugar dehydration, s^{-1}	Y_{eq}	equilibrium absolute humidity of air at the grain surface, kg water/kg dry air
K	total solids moisture and air vapor content in an element, kg	Y_s	saturated absolute humidity, kg water/kg dry air
L_h	latent heat of water vaporization, J/kg	α	constant in Eq. (14)
m_a	mass of air in an element, kg	$\gamma_1, \gamma_2, \gamma_3$	constants in Eq. (14)
m_s	mass of sugar in an element, kg	ΔT	amplitude of temperature square wave, °C
N	number of particles in unit volume		
P	ambient pressure, Pa	ΔV	elemental volume in the domain containing solid and gas, m^3
r, z	cylindrical coordinates, m		
R	radius of sugar particle, m	ε	porosity of granulated sugar
RH	relative humidity of air	θ	polar/cylindrical coordinate
R_v	individual gas constant for water vapor, J/kg K	λ_s	thermal conductivity of granulated sugar, J/s m°C
t	time, s	ξ	dimensionless geometry-dependent coefficient
T	temperature of air or granular sugar, °C	ρ_a	density of air, kg/m^3
T_i	initial temperature of granular sugar, °C	ρ_s	solid density of granulated sugar, kg/m^3

1. INTRODUCTION

Sugar production is seasonal. However, its consumption is actually evenly distributed over the whole year. Hence, large quantities of sugar must be stored in bags and bulk storage in silos or storage bins and distributed in chain. Because of the rapid method of drying, an excess of moisture is trapped in the center of the particle and produces a glassy layer of amorphous sugar [1–4]. Some of this moisture becomes part of the crystal structure, called inherent moisture in a thermodynamically stable crystal state. The rest of the moisture can exist in an amorphous state, which is not at true stable equilibrium. The stickiness and state changes of amorphous sugar are often related to its glass transition temperature. The transition temperature is dependent on the moisture content and temperature. This can be best seen by a state diagram which defines the moisture content and temperature region at which the sugar domain is glassy, rubbery, crystalline, frozen, etc. [4], and changes in the amount of moisture in the amorphous state can affect the physical state and quality of the sugar crystal. Hence, an understanding of moisture migration and moisture

sorption or desorption by sugar is of prime importance, since many physical and chemical properties such as caking, plasticization, and dehydration are functions of both the sugar moisture content and water activity.

Moisture movement through unsaturated food particles is often caused by changes of ambient temperature. Water evaporates from hot regions and moves across the gas-filled pores by diffusion and condenses on the colder regions, thus releasing its latent heat of vaporization. Consequently, at least two main aspects of coupled heat and mass transfer should be included: (1) moisture loss or gain in a given food component and (2) moisture migration driven by temperature and concentration gradients between different regions.

In the past few years, many investigations on coupled heat and mass transfer have been carried out in a wide range of engineering domains, for food engineering [1–4], geothermal engineering [5–7], drying technology [8–10], and others [11–13], both theoretically and experimentally. A phenomenological theory of combined heat and mass transfer in porous media was previously established by Philip and DeVries [5] and DeVries [14], in which the transport due to capillary forces was represented in terms of gradients of the moisture content and temperature. Similar equations for heat and mass transfer in porous media were also published by Luikov [15]. The modeling of heat and mass transfer has been recently revisited, based on its initialization at the pore level [6]. The homogenization method is applied to porous media by using the volume averaging method, in which the periodic medium is assumed to stand for an elementary representative volume (ERV). Then, the modeling is obtained by using asymptotic expansions for the periodic medium. A number of researchers have applied Luikov's equation to solve the two-way coupled [16, 17] and three-way coupled equations [18]. The finite-volume method [16] and the finite-element method [17, 18] were employed in their researches. Several researchers have used pore network modeling to simulate drying processes in capillary porous media [8, 10] and diffusion in chromatography [11]. Pore network models are based on a network representation of the porous structure. The pores are the network nodes associated with the ''sites'' of percolation networks through the throats of their connecting ''bonds.'' The mass in liquid-filled and gas-filled pores is conserved by Kirchoff's current law. Pore network models are then used to compute the effective parameters as a function of transport scales. The pore network models have been successfully applied to the simulation of the dry patch phenomenon and the constant-drying-rate period [8, 10].

The common feature of all the above works is that both a microscopic and a macroscopic description of mass balances have been carried out. The two balances are connected through the volume averaging technique. However, the above researchers focused mainly on nonhygroscopic materials. Moisture was merely trapped in the gaps between the solid particles. The solid material did not absorb moisture, and the effect of solids moisture was neglected. In practice, many materials (such as textile fiber, food, soil, etc.) have a certain degree of moisture absorption/desorption capability.

For these hygroscopic materials, moisture is not merely trapped in spaces between the solid particles but may be bound to solids which exhibit energetic retention of moisture. The free energy of the moisture–solid bond rises as relative humidity decreases. Therefore, knowledge of the interaction between moisture and

solid is an essential prerequisite in order to determine changes in moisture. However, our present theoretical understanding does not enable us to derive the relationship between the equilibrium moisture content and the relative humidity from first principles because of the complexity of absorption and desorption processes of materials. Solution of the macroscopic equations for heat and mass transfer at conditions of full saturation may yield satisfactory answers in one-way processes (as is the case, i.e., in [9], where the drying process of softwood is described with the solids moisture content being linearly related to temperature), but equilibrium thermodynamics suggest that solids moisture contents cannot be related to temperature through a simple linear equation, especially when saturation has not been reached and the equilibrium balance is very unstable. An alternative approach is to employ semiempirical relationships of equilibrium moisture contents of materials through experiments. Then, these semiempirical relationships are integrated into the coupled heat and mass transfer equations. In recent years this approach has been adopted by most researchers. Sorption isotherms have been utilized to account for the dependence of sugar moisture on relative humidity in order to simulate heat and mass transfer in sugar silos [1]. Also, the heat and moisture transfer with sorption and condensation in porous clothing assemblies was investigated by employing an experimental relationship between moisture concentration of fibers and relative humidity [12]. However, these works neglected the influence of temperature on the sorption/desorption process. Experimental data have confirmed that the sorption/desorption of moisture is affected by temperature [19]. Moreover, these works did not consider the effect of temperature and moisture content on the thermal conductivity and mass diffusion coefficient. Molenda et al. [20] derived a vapor–moisture–temperature relationship which neglected the hysteresis of absorption isotherms by using Maulem and Dagan's model III. In this relationship, there are two undetermined functions, $F_c(\Omega)$ and $G(\Psi)$, which are dependent on the main hysteresis cycle and a primary draining curve. Unfortunately, a general theoretical expression based on the thermodynamic law is not given for these two undetermined functions. Empirical expressions based on experimental data must still be employed to bring closure to the problems considered. Clearly, our understanding of coupled heat and mass transfer in hygroscopic materials in engineering applications is still not adequate, and further investigations are required.

The aim of this article is to develop a mathematical model to describe heat and moisture transfer with phase change. This includes source terms which account for absorption and desorption and have been derived on the basis of microphysics. An equation for the mass diffusion coefficient as a function of temperature has been incorporated into the model. Additionally, the mathematical model was developed in order to predict the distribution of moisture concentration driven by the temperature cycling. The present work focuses on the effects of cycling temperature variations on the subsequent moisture migration. A highly conductive, impermeable boundary has been assumed between the material and the ambient environment, where no moisture was allowed to penetrate into or out of the system. Experimental investigations on sealed granulated sugar bags were performed, where moisture migration is driven only by temperature gradients, and the results were compared against the predictions of the model. Predictions then follow about the effects of varying boundary conditions on the migration of moisture in the simulated system.

2. THEORETICAL MODEL

2.1. Heat and Mass Balance Equations and Initial and Boundary Conditions

The schematic diagram of an infinitely long cylindrical sugar bag, where the temperature of the exposed surface is varying periodically with time, and the computational domain which is employed to model coupled heat and moisture transfer through sugar bulk, are shown in Figure 1*a*. Due to the symmetrical nature of the problem, the computational domain represents a one-dimensional "slice" of 5° of the cylindrical bag. The outer layer of the cylinder consists of a polyethylene-lined bag, of 0.5 mm thickness. For the construction of the mathematical model, the following assumptions have been taken into account:

Sugar in the macroscopic sense is considered to be homogenous and isotropic.
Hysteresis in the relation between the moisture potential and the moisture content is not taken into account.
Local thermal and moisture equilibrium exists among all phases.
Shrinkage and swelling effects are neglected as solid absorbs and desorbs moisture, so that the porosity remains constant.
Convection and radiation transport phenomena are negligible compared with diffusion.
The polyethylene is not permeable and does not allow moisture to diffuse in or out of the system.
Ambient pressure is constant.

Based on the above assumptions and the cylindrical coordinate system in Figure 1, the one-dimensional governing partial equations of heat and mass transfer are given as follows.

1. *Energy conservation:*

$$(1-\varepsilon)\rho_s c_{ps}\frac{\partial T}{\partial t} = \frac{1}{r}\frac{\partial}{\partial t}\left(\lambda_s r\frac{\partial T}{\partial r}\right) + L_h(1-\varepsilon)\rho_s\frac{\partial W}{\partial t} \tag{1}$$

where c_{ps} and λ_s are the specific heat capacity and thermal conductivity for granulated sugar, respectively, L_h is the latent heat of water vaporization, ε is the fraction of the total volume of the package occupied by air (i.e., porosity), and W is the moisture content of the solid (in %, representing the mass of liquid water in the solid).

2. *Mass conservation:*

$$\frac{\partial Y}{\partial t} = \frac{1}{r}\frac{\partial}{\partial r}\left(D_e r\frac{\partial Y}{\partial r}\right) - \frac{(1-\varepsilon)\rho_s}{\varepsilon\rho_a}\frac{\partial W}{\partial t} \tag{2}$$

where D_e is the effective diffusion coefficient for water vapor in air. Y is dimensionless and represents the mass of water vapor in the air around the solid particles. Equations similar to Eqs. (1) and (2) can be obtained by using the volume averaging method with the grain scale description [6].

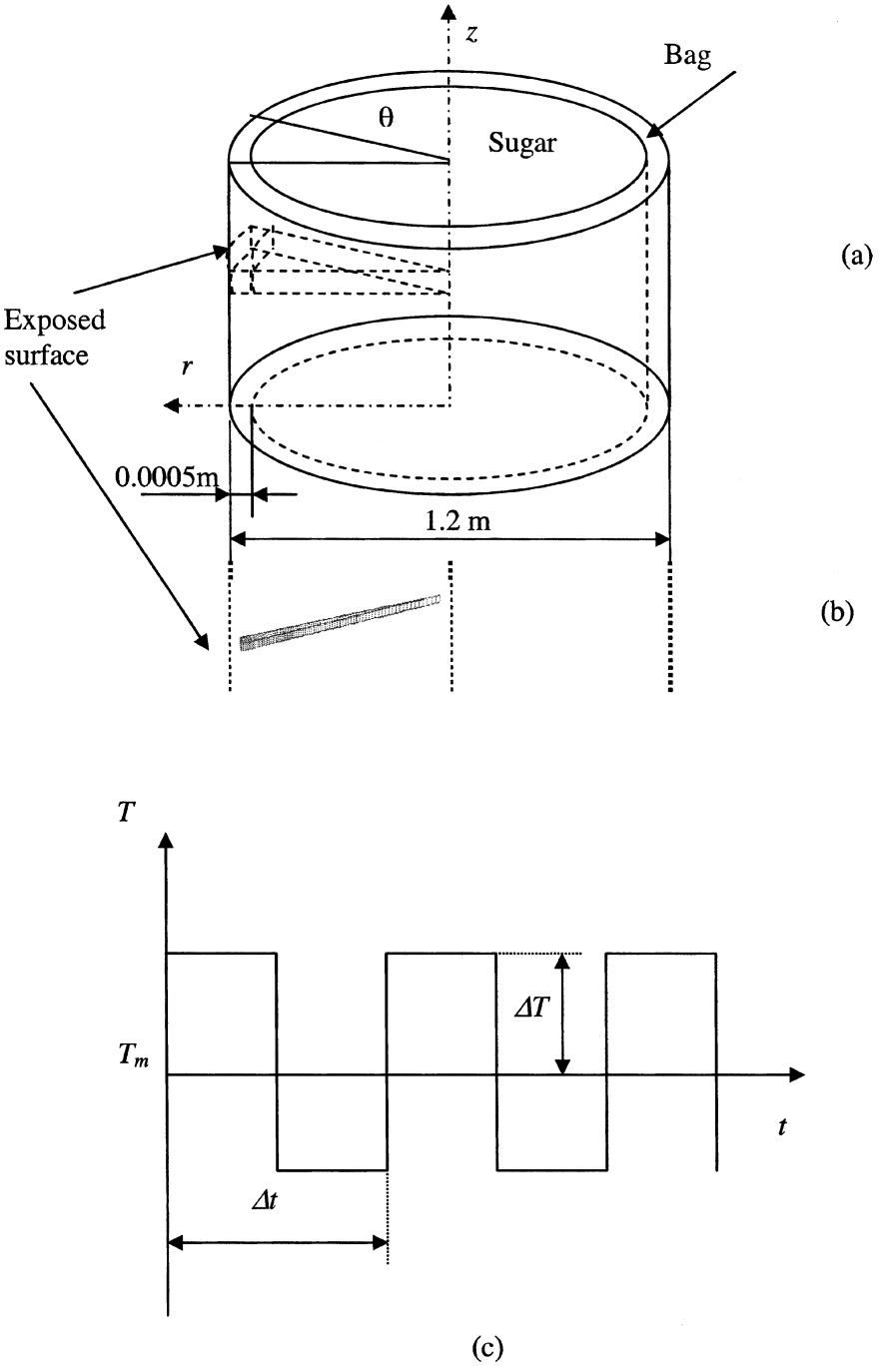

Figure 1. Schematic representation of (*a*) simulated sugar bag and (*b*) computational domain and mesh, and (*c*) square-waveform temperature profile at the boundary.

3. *Initial and boundary conditions*:
Initial conditions:

$$T = T_0, W = W_0, \quad \text{and} \quad Y = Y_0 \quad \text{at } t = 0 \tag{3}$$

Boundary conditions: At the center of the sugar bag and along the z direction, free-slip boundaries are assumed, due to the symmetry of the problem. No moisture is allowed to penetrate into/out of the system through the bag, and the only interaction allowed with the environment is through changes of the environmental temperature, which affect the material via heat conduction through the polyethylene layer. Hence, Eq. (1) needs to be solved for the bag, where the bag thermal properties and density have to substitute for the granulated sugar properties (i.e., for polyethylene, specific heat capacity 4,120 J/kg°C, thermal conductivity 5 J/s m°C, and density 1,192 kg/m^3). The initial boundary conditions can be summarized as

$$\begin{aligned} T\big|_{r=r_0} &= T_s \qquad \left.\frac{\partial Y}{\partial r}\right|_{r=r_0} = 0 \\ \left.\frac{\partial T}{\partial r}\right|_{r=0} &= 0 \qquad \left.\frac{\partial Y}{\partial r}\right|_{r=0} = 0 \end{aligned} \tag{4}$$

Equations (1) and (2) are highly nonlinear and coupled to each other through source terms. The temperature of the exposed surface varies periodically with time. The time-varying temperature patterns are square-wave profiles with different mean temperature and oscillation amplitude, as shown in Figure 1*c*.

2.2. The Effective Diffusion Coefficient

The effective diffusion coefficient of vapor in the air around the sugar granules is the product of the porosity and the diffusion coefficient of vapor in dry air, D_a. By employing the formula for D_a (which is a function of temperature and pressure, [21]) the effective diffusion coefficient can be expressed as follows:

$$D_e = \varepsilon \cdot 2.11 \times 10^{-5} \left(\frac{273.15 + T}{273.15}\right)^{1.94} \left(\frac{1013.25}{P \cdot 10^{-2}}\right)^2 \tag{5}$$

where T is in °C and P is in Pa.

For the present case, the ambient pressure may be considered as constant, and is equal to atmospheric pressure. Therefore, the above equation may be simplified as

$$D_e \approx \varepsilon \cdot 2.11 \times 10^{-5} \left(\frac{273.15 + T}{273.15}\right)^{1.94} \tag{6}$$

2.3. Source Terms

The source terms in Eqs. (1) and (2) represent the increase or decrease in temperature due to the release or absorption of heat during condensation or evaporation, respectively, and the subsequent decrease or increase in the mass of vapor in the air around the solid particles. These source terms are related to the moisutre production or destruction on solid particles at the micro scale, and should take into account the solid gas and (air + vapor) phases, the solid bound moisture, and the thin layer of liquid syrup around the particles, which results from the condensation of vapor on the particle surface. A schematic representation of the region between sugar granules in the bag is given in Figure 2. The total flux of moisture from/onto the solid surface depends on the concentration gradients, the mass transfer rate, and the area of solid–air interface and represents the production/destruction of the solid matrix. In this way, the net mass transfer flux of moisture is obtained on the basis of the following micro-mass balance:

$$(1-\varepsilon)\rho_s \frac{\partial W}{\partial t} = \frac{\varepsilon \rho_a \xi D_a}{F}(Y_{\text{eq}} - Y) \tag{7}$$

where F is the area of solid–air interface in an elemental volume ΔV, Y_{eq} is the equilibrium absolute humidity at the grain surface, ξ is a dimensionless geometry-dependent coefficient, and D_a is the diffusion coefficient of vapor in dry air. As an approximation, F is equal to the sum of all particle surfaces:

$$F = NA$$

where N is particle number in the elemental volume, which is equal to the total solids volume in an element divided by a single particle volume:

$$N = \frac{(1-\varepsilon)\,\Delta V}{V}$$

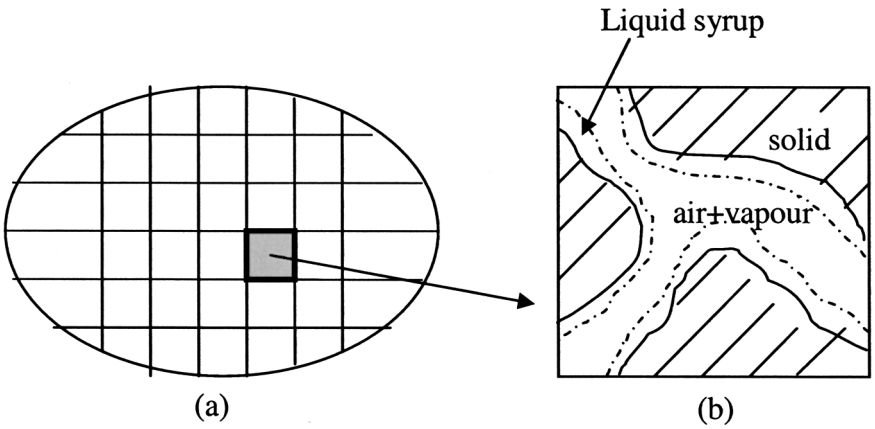

Figure 2. Schematic diagram of periodic pore space in porous media: (*a*) macroscopic, and (*b*) microscopic views.

and A is the surface area of a single particle. Assuming spherical particles of an average radius R, A and V are given by $A = 4\pi R^2$ and $V = \frac{4}{3}\pi R^3$. Substituting N, A, and V into Eq. (7), the following expression is derived:

$$(1-\varepsilon)\rho_s \frac{\partial W}{\partial t} = -\frac{\varepsilon \rho_a \xi R D_a}{3(1-\varepsilon)\Delta V}(Y_{\text{eq}} - Y) \tag{8}$$

Based on Eq. (8), a mass transfer coefficient k can be defined as follows:

$$k = \frac{\xi R D_a}{3(1-\varepsilon)\Delta V} \tag{9}$$

Thus, Eq. (8) may be written as

$$(1-\varepsilon)\rho_s \frac{\partial W}{\partial t} = -\varepsilon \rho_a k(Y_{\text{eq}} - Y) \tag{10}$$

where, following [15],

$$Y = \text{RH} \cdot Y_s = \text{RH} \cdot \frac{C_1 e^{-C_2/(273.15+T)}}{\varepsilon \rho_a R_v (273.15 + T)} \tag{11}$$

The term $C_1 e^{-C_2/(273.15+T)}$ in Eq. (11) is derived through the Clausius-Clayperon equation for the equilibrium between vapor and liquid phases of water and describes the dependence of saturation vapor pressure on temperature [22]. For its derivation, latent heat of vaporization has been approximated as a constant (its relative variation between a range of temperatures of -5°C and $+40$°C is of the order of less than about 4.7%), and integration of the Clausius-Clayperon equation between a temperature T and a temperature $T_0 = 0$°C has been performed. The term C_1 is related to the saturation water vapor pressure at 0°C, which can be considered as constant [22], while the term C_2 is related to the ratio of the latent heat of vaporization at 0°C to the individual gas constant for water vapor. For a more detailed analysis of the Clausius-Clayperon equation and the subsequent derivation of this term, the reader is referred to [22].

Hence:

$$Y_{\text{eq}} = \text{ERH} \cdot Y_s = \text{ERH} \cdot \frac{C_1 e^{-C_2/(273.15+T)}}{\varepsilon \rho_a R_v (273.15 + T)} \tag{11a}$$

In practice, the particles are not regular spheres of equal radii; liquid bridges can form between particles, hence reducing the porosity. All undetermined factors have been incorporated into the dimensionless geometry-dependent coefficient, ξ. Since there can be no direct measurements of the mass transfer coefficient [1], the parameter ξ has to be calibrated to experimental data for a particular material, in order to fit the sorption/desorption behavior of that material. It is interesting that Eq. (8) is very similar to the expressions employed in [1], [23], and [24] to describe the rate of change of the solids moisture content.

2.4. Equilibrium Absolute Humidity of Air at the Grain Surface

The total amount of moisture within a control volume must be balanced. As the temperature changes, the relative humidity of the air is changed, and this results in disturbing the equilibrium of the system. Consequently, either vapor will be absorbed by the grains or evaporation from the grain surface will occur, so that the system again reaches equilibrium. Hence, the moisture balance in a control volume can be obtained as follows:

$$K = m_a \cdot Y + \frac{m_s W}{100} \tag{12}$$

where, following Eq. (11), $Y = \mathrm{RH} \cdot Y_s$. Hence, at equilibrium, Eq. (12) may be rewritten as

$$K = m_a \cdot \mathrm{ERH} \cdot Y_s + \frac{m_s W_{\mathrm{eq}}}{100} \tag{13}$$

The semiempirical relationship between W_{eq} and ERH for granulated sugar can be obtained from experimental data [19]:

$$W_{\mathrm{eq}} = (\gamma_1 + \gamma_2 \mathrm{ERH}^{\gamma_3}) \left(\frac{T}{20}\right)^{\alpha} \tag{14}$$

Substituting Eq. (14) for W_{eq} into Eq. (13), the equilibrium relative humidity can be obtained through the solution of the quadratic

$$\frac{m_s \gamma_2}{100} \left(\frac{T}{20}\right)^{\alpha} \mathrm{ERH}^2 + m_a Y_s \,\mathrm{ERH} + \frac{m_s \gamma_1}{100} \left(\frac{T}{20}\right)^{\alpha} - K = 0 \tag{15}$$

where $\gamma_1, \gamma_2, \gamma_3$, and α are dimensionless constants, specific to granulated sugar, as given in [19]. K may be calculated via Eq. (12) (where the current values of Y and W may be used) and Y_s can be obtained following [21]:

$$Y_s = \frac{C_1 e^{-C_2/(273.15+T)}}{\varepsilon \rho_a R_v (273.15 + T)}$$

Numerical tests were performed in order to calibrate ξ to experimentally determined sorption/desorption curves for granulated sugar [19]. It was found that a range of values for ξ, between 0.7 and 1.4, adequately fitted the sorption/desorption behavior of the material with a maximum deviation of approximately 12%. The width of this range could be attributed to the fact that the diffusion terms in the heat and mass transfer equations are still dominant, compared to the source terms. Hence, in this study, ξ was taken to be unity, an approximation which, as will be demonstrated, was adequate to represent the behavior of granulated sugar during varying environmental conditions.

3. SOLUTION PROCEDURE AND NUMERICAL CONSIDERATIONS

The governing equations are discretized using the finite-volume method [25, 26]. The central-difference scheme is used for interpolation since there are no convective terms. Nonuniform hexahedral cells are employed in this article. The mesh used is shown in Figure 1.

After discretization, the linearized set of Eqs. (1) and (2) and boundary conditions can lead to two tri-diagonal matrix equations, one for T and one for Y. The two matrix equations are coupled through the source term. The solution procedure has been implemented within PHYSICA, a three-dimensional, fully unstructured, fluid dynamics/solid mechanics finite-volume code, developed at the University of Greenwich [27]. The equations have been solved numerically using the PHYSICA solvers, which employ overrelaxed Jacobi (JOR) and overrelaxed Gauss-Seidel (SOR) techniques [27]. However, complete elimination of nonlinearities in Eqs. (1) and (2) is not possible, due to the fact that the effective diffusion coefficient and source term are nonlinear functions of temperature and absolute humidity. Hence, an iterative procedure must be employed. This procedure involves the following steps: (1) start with initial temperature and absolute humidity; (2) using these starting values, an equilibrium absolute humidity can be calculated, which is then used to update temperature and moisture content; (3) update absolute humidity using the updated values of equilibrium absolute humidity and moisture content; (4) return to step 2 and repeat the calculation procedure using the updated values of temperature and absolute humidity until convergence is achieved for all solved parameters. Thermodynamic and transport properties can be updated simultaneously, as the solution is iterative.

It should be noted that when the source term is too big, the tri-diagonal matrix becomes unstable. To improve the stability of solution, a small time step should be used, or the source term must be linearized in some suitable fashion [25, 26].

4. RESULTS AND DISCUSSION

Typical granulated sugar and air properties and associated thermodynamic and transport parameters are given in Table 1. The granulated sugar particles contained in the simulated bag were of an average diameter of 0.6×10^{-3} m. The initial absolute humidity was taken to be (assuming that the system was initially at equilibrium) $Y_0 = 0.0220$ kg/kg at $W_0 = 0.068\%$ and $T_0 = 18°\text{C}$ (W_0 and T_0 were measured values). These initial conditions were employed in all of the performed simulations, unless otherwise stated. A nonpermeable boundary of moisture was

Table 1. Simulation constants of thermodynamics and transport properties

λ_s	ρ_a	ρ_s	c_{ps}	L_h	C_1	C_2
0.208	1.293	1,600	2,087.3	2.272×10^6	2.53×10^{11}	5.42×10^3
J/m s°C	kg/m^3	kg/m^3	J/kg°C	J/kg	Pa	K
R_v	ξ	ε	α	γ_1	γ_2	γ_3
461.5 J/kg K	1	0.4164	0.6	0.03	0.075	2

assumed, since the permeability of polyethylene was very small (1×10^{-9} kg m^2/s). Hence, in the bag lining, only the energy equation was solved, where the polyethylene properties (i.e., thermal conductivity, specific heat capacity, density) were considered.

A number of initial numerical tests were performed to assess the effect of the mesh size and time step on the results. It was found that for meshes with 50 to 90 elements for a 10-s time step, or a 90-element mesh for 40 s at 10-s time steps, the difference in the iteratively solved parameters (i.e., temperature, absolute humidity, solids moisture content) was of the order of 0.9% or less. Since the simulated problem is essentially one-dimensional and does not require excessive CPU time to run, a 90-element mesh and a time step of 10 s were chosen for the simulations performed. The CPU time required for simulating 240 h of a temperature cycling process on a Digital Unix Alpha 466-MHz processor was of the order of 18 h.

Numerical results were first validated against experimental data in [19, 28]. The comparisons between experimental data and predictions are made and analyzed in terms of temperature profiles. Then, moisture migration profiles driven by temperature gradients are calculated and analyzed within the sugar bulk in big bags.

A typical time-varying square-wave temperature profile, employed to evaluate the impact on moisture migration, is given in Figure 1*c*.

4.1. Comparison between Predicted and Experimental Data

Figure 3 shows a comparison of temperature profiles between experimental data and the model predictions. A bag of granulated sugar 60 cm in diameter was subjected to temperature cycling in a humidity cabinet, where it was ensured that the top and bottom of the bag were thermally insulated, so that the only interactions between bag and environment occurred through the sides of the bag [28]. The initial temperature of the system was 18°C. Then the ambient temperature was raised to 40°C and kept constant for 48 h. The predicted temperature profiles are shown in Figure 3*a*. for the first 4 h. It can be seen that the temperature near the bag–sugar boundary rose gradually with time. However, the core temperature remained unaffected during the first 4 h. This is due to the low thermal conductivity of granulated sugar, which will increase the response time of the material to environmental temperature variations. Corresponding experimental results are shown in Figure 3*b*.

Further detailed comparison between predicted and experimental results at $t = 4$ hours are shown in Figure 3*c*. The results presented show very good agreement between experiment and numerical simulation. The maximum deviation between the predicted and experimental results did not exceed 2°C. It should be noted that experimental measuring accuracy of the thermocouple probes used is of the order of $\pm 1\%$.

Experiments which examine moisture migration trends in solids are time-consuming and often very complicated to perform, hence not enough experimental data under carefully controlled conditions are available in the literature. In [19], experiments were performed which measured the moisture uptake by granulated sugar under controlled temperature variations. Granulated sugar, directly after conditioning, was placed in a caking box, which was impermeable to the environmental moisture and hence did not allow any moisture to enter/leave the system. The

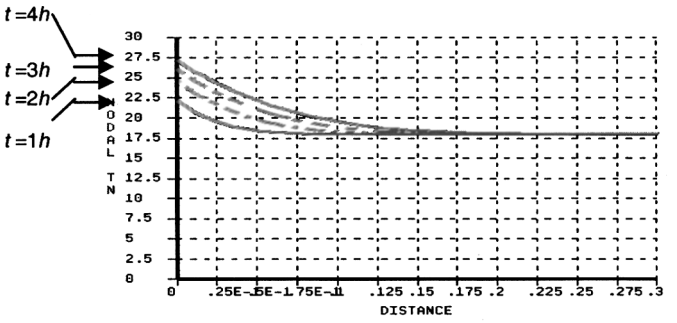

(a)

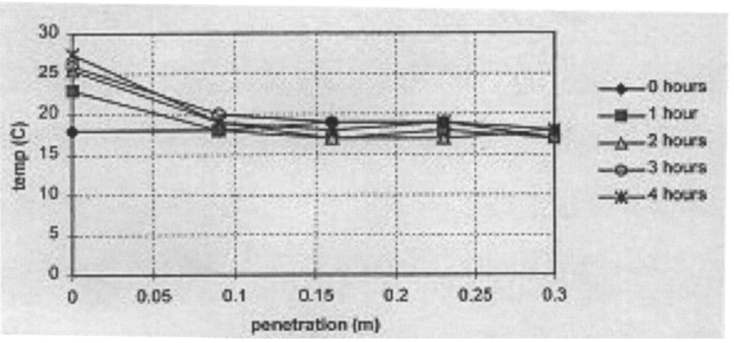

(b)

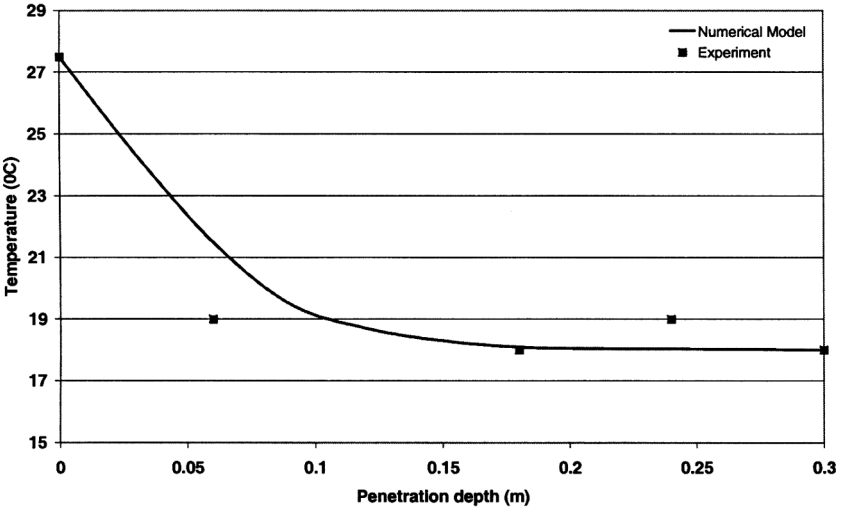

(c)

Figure 3. Comparisons between (*a*) model predictions and (*b*) experimental data (Leaper et al. [28]) to study the effect of a constant environmental temperature on the penetration depth in a bag which contains granulated sugar; and (*c*) further detailed comparison at $t = 4$ h when the exposed surface temperature rises to 40°C for 4 h.

box allowed heat conduction only in one dimension, through one surface fitted with platens, and was thermally insulated on all other sides. Initially, the material temperature was 20°C, its relative humidity was 45%, and the solids moisture content was 0.051%. The sugar properties were as given in Table 1. First, the temperature of the platens was dropped to 10°C for 12 h and then it was increased to 30°C for a further 12 h. Then, the box was placed in an oven with dessicant at 45°C for 2 weeks (i.e., one-dimensional heat conduction process through the noninsulated surface) and readings of the material moisture content were taken at the end of this process. The numerical model simulated the experimental process, and a comparison between the model predictions and the experimentally measured values for the sugar moisture content at the end of the process is shown in Figure 4. As can be seen, there was very good agreement between model and experiment, with the model accurately predicting, both qualitatively and quantitatively, the moisture migration behavior in the solid. The maximum deviation between measured and predicted values was less than 4%, a value which was well within the range of ±4% uncertainty of the experimental measurements.

4.2. Numerical Simulation of Heat, Absolute Humidity, and Moisture

As environmental temperature changes periodically with time, the dynamic profiles of temperature, absolute humidity of air, and moisture contents of sugar are shown in Figure 5. A sugar bag, as described in Figure 1, was simulated with the environmental temperature rising first at 40°C and kept constant for 12 h and then

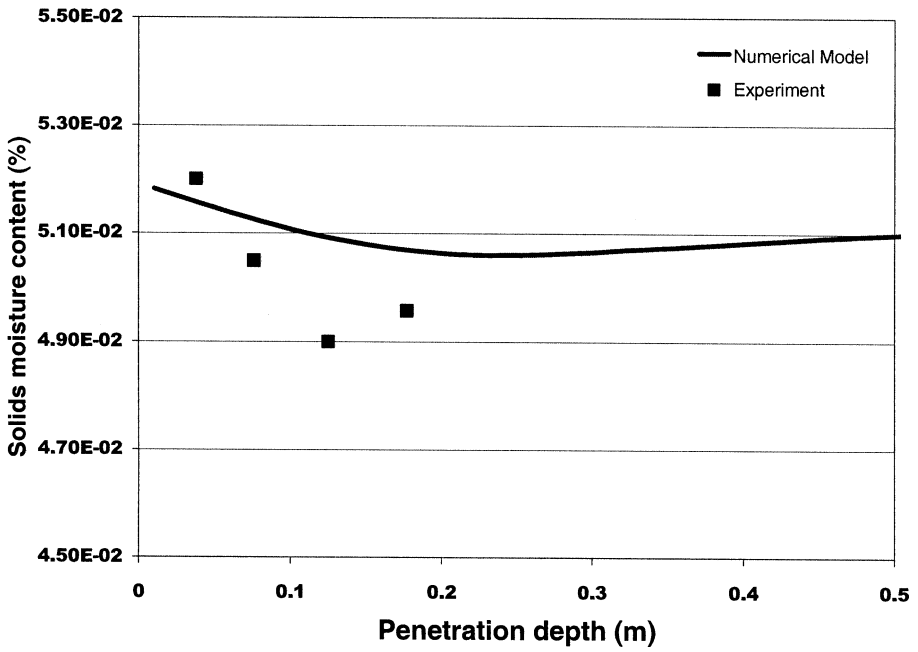

Figure 4. Comparison between experimental data and numerical model predictions for the solids moisture content at different penetration depths after a 15-day-long process.

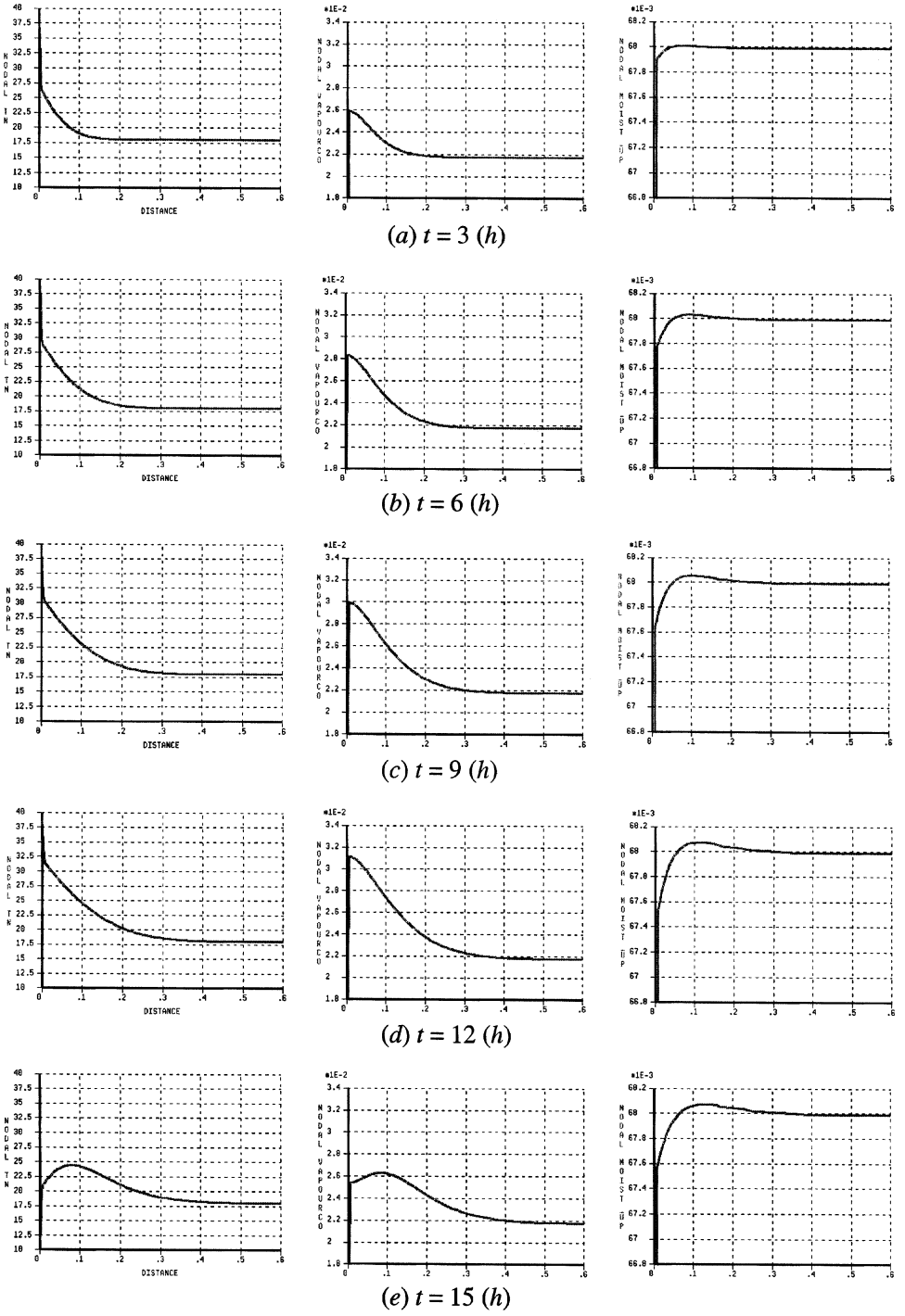

Figure 5. Profiles of temperature (*left*), absolute humidity (*middle*), and moisture content (*right*) at penetration direction for the first 30 h of a cyclic process of ten 24-hour cycles.

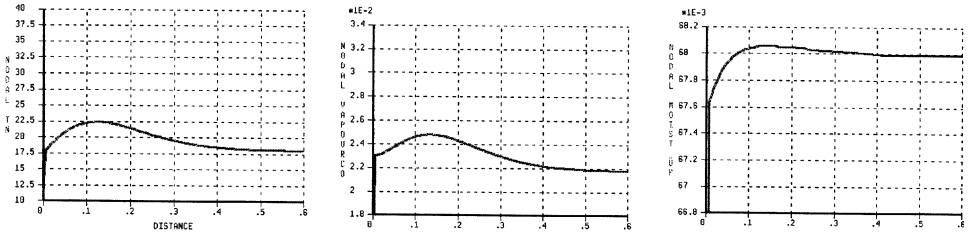

(*f*) $t = 18$ (*h*)

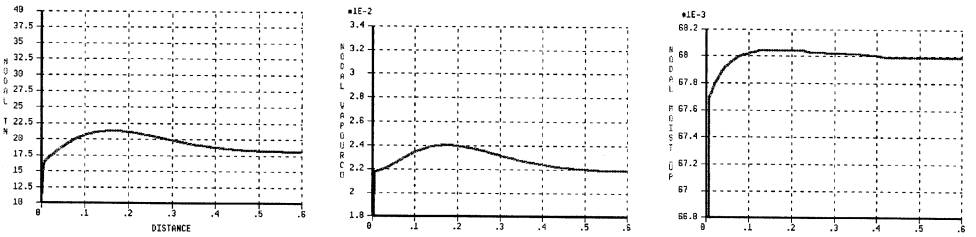

(*g*) $t = 21$ (*h*)

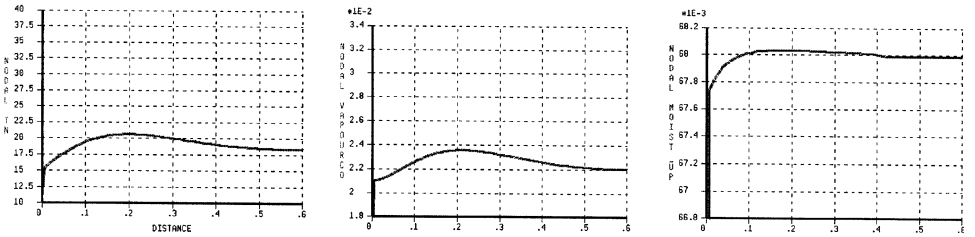

(*h*) $t = 24$ (*h*)

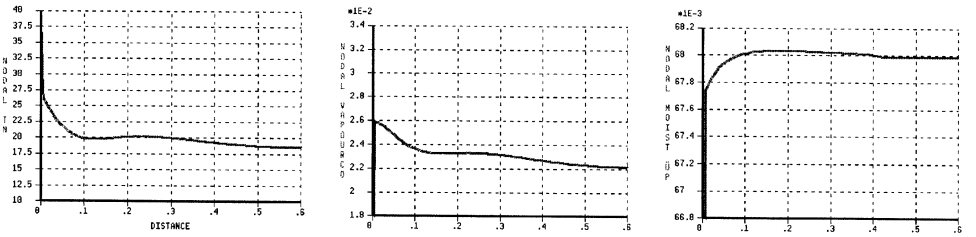

(*i*) $t = 27$ (*h*)

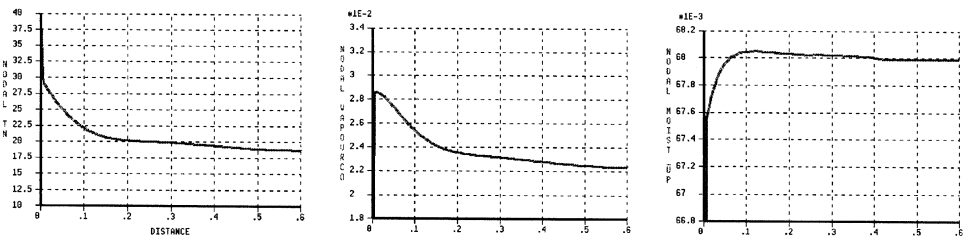

(*j*) $t = 30$ (*h*)

Figure 5. (Continued).

dropped to 10°C and kept constant for a further 12 h. The process was repeated for a further nine 24-h cycles. In Figure 6, numerical results for the first 30 h are presented, where the left panel shows temperature, the middle panel absolute humidity, and the right panel solid moisture content.

Figures 5*a*–5*d* show the response of temperature, absolute humidity, and moisture content to the environmental temperature rising. It can be seen that when

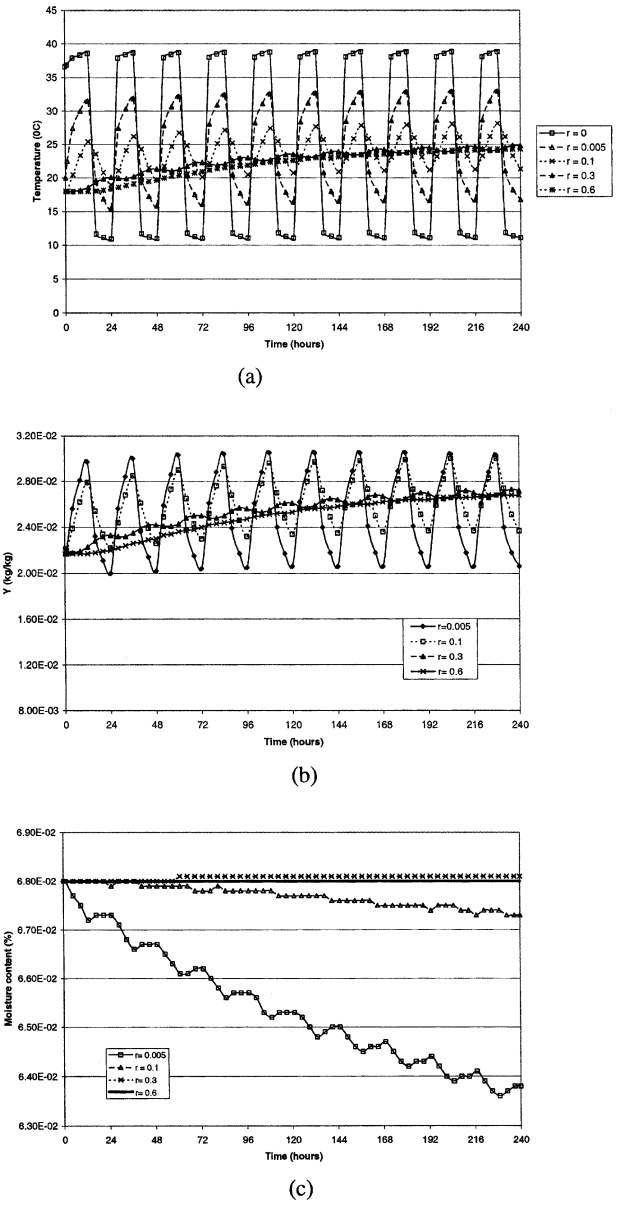

Figure 6. Variation of (*a*) temperature, (*b*) absolute humidity, and (*c*) moisture content profiles with time and penetration distance, *r*, under oscillating environmental temperature conditions.

the ambient temperature rose to 40°C, there was an almost instantaneous increase of temperature within the bag layer, due to the polyethylene being highly conductive. Within the sugar, the temperature decreased along the penetration distance, with the region in the core remaining almost unaffected. The corresponding absolute humidity was seen to increase near the bag–material interface, while the moisture content was seen to decrease. This is due to the fact that the temperature increase triggered a decrease in the relative humidity of the air in that part of the domain, hence making the system deviate from its equilibrium state. In its attempt to drive the system back to equilibrium, moisture had to evaporate from the solid in order to replenish the vapor content of the air. Hence, the moisture of the solid was seen to decrease, with a simultaneous increase of the absolute humidity of the air. Thus, a concentration gradient of absolute humidity was produced in the system, which would tend to drive the absolute humidity from the bag–material interface toward the core of the bag. This increase in absolute humidity would then break the equilibrium of the system farther away from the boundary, by increasing the relative humidity of the air, and the system, in its attempt to reach equilibrium again, would then condense some of the excess vapor of the air onto the solid, thus increasing its moisture content away from the environment–bag boundary. Hence, the process of moisture migration is established, driven by both temperature and absolute humidity gradients. It is interesting to note that changes in absolute humidity and solids moisture content were confined within a distance of approximately 0.2 m from the bag–environment boundary. This is in agreement with the observed temperature penetration depth of approximately 0.2 m, which was also confirmed experimentally from the results presented in Section 4.1. Beyond that point, the system remained in thermodynamic equilibrium.

Figures 5*e*–5*h* present the results when the boundary temperature dropped to 10°C. Again the temperature inside the bag layer dropped almost instantaneously to 10°C, due to the high conductivity of polyethylene. Within the sugar, the temperature was seen to decrease from central regions toward the bag–environment boundary, with the sharpest decrease being at the bag–material interface. The opposite process from the one described previously, when the temperature rose to 40°C, would occur, with the absolute humidity close to the bag–material interface decreasing and the solids moisture content increasing (due to the increase in the relative humidity of the air in that region, and the subsequent condensation of the excess vapor on the sugar particles). The absolute humidity gradient between the core and the bag–material interface would tend to decrease the absolute humidity further inside the bag (around the region at a distance of 0.2 m from the bag–environment interface), which would then cause the relative humidity in that region to decrease, hence causing the evaporation of moisture from the solid interface in order for the system to return to equilibrium. Hence, in this case, moisture would be seen to migrate from the core toward the bag–sugar interface.

Figures 5*i*–5*j* present the initial stages of a new cycle, with the environmental temperature being raised again to 40°C. As was expected, the process of moisture migration from the bag–material interface toward the central regions was starting to take place once more, caused by changes in temperature and absolute humidity.

Figure 6*a* presents the system thermal response to the changes of environmental temperature at various penetration distances along the simulated

environment–bag central core domain. It can be seen that the bag polyethylene lining responded immediately to the external fluctuations. Temperatures in inner layers were observed to behave in a sawtooth fashion. The amplitudes of these sawtooth patterns decreased with increasing distance from the bag–environment boundary. Finally, the amplitudes of the sawtooth seemed to become very small at the center of the bag. It can also be seen that there was a slow increase in the central-region temperature with time, until the oscillating temperature average of 25°C was reached. This phenomenon was due to the fact that the temperature gradients between the bag core and intermediate regions were always smaller than between the bag–environment interface and the intermediate regions, hence the changes in temperature were not sharp in the core and the tendency of the system would be to attain an equilibrium state around the oscillating temperature average of the process.

Figure 6*b* shows that the absolute humidity exhibits similar behavior to that of temperature. As discussed either, changes in temperature will result in changes to the system relative humidity and deviation from its equilibrium state, which will result in evaporation (temperature increasing)/condensation (temperature decreasing) on the sugar grain surface with subsequent increase/decrease of the absolute humidity in order for the system to be driven back to equilibrium. The absolute humidity was seen to vibrate with the changing temperature pattern. The amplitudes of vibrations decreased toward the core regions, with the absolute humidity tending to its equilibrium value at 25°C.

Figure 6*c* shows the behavior of the solids moisture content at various penetration levels from the environment–bag boundary. The sharpest oscillations seemed to occur around the sugar–bag interface, where the sharpest oscillations in temperature and absolute humidity occurred. Moisture migration was predicted to occur within the first 0.2 m of penetration depth. When the boundary temperature was increasing, moisture seemed to migrate from the bag–material interface toward the intermediate bag regions (around 0.2 m depth), and when the temperature was decreasing the opposite process was taking place. The amplitude of the oscillations decreased toward the core of the bag. An interesting observation was that the trend for the solids moisture close to the material–bag interface was to decrease, which is in line with the results presented in Figures 6*a* and 6*b*, where the temperature and absolute humidity were seen to increase close to the bag core. Since the bag–environment boundary was impermeable to moisture, the total amount of vapor/liquid in the domain should be conserved. Therefore, since there was an increase in the air vapor content (i.e., increase in absolute humidity) in the central regions, there should be a decrease in the solids moisture content in a part of the domain. This decrease would not have been expected to occur in the moisture content of the solids close to the core of the bag. As the temperature rise in the bag core occurred gradually and in a smooth manner, the system had time to achieve equilibrium in this region through the diffusion of water vapor from intermediate bag regions. In this way, the equilibrium absolute humidity was not very different from the ambient-air absolute humidity at every stage of the process, so that the change in the solids moisture content in the core region was very small. Therefore, the conservation of total vapor/moisture content should come through the decrease in the solids moisture content of regions where the temperature/absolute humidity gradients are the sharpest, thus affecting the equilibrium humidity of the system (i.e., close to the bag–material interface).

4.3. The Effect of Temperature Oscillation Amplitudes on Heat and Mass Transfer

Simulations were then performed with the same initial conditions and oscillating temperature average T_m at 25°C but with different amplitudes, namely, 10°C (temperature oscillating between 35°C and 15°C) and 20°C (temperature oscillating between 45°C and 5°C). As before, ten 24-h cycles were simulated, with the external boundary being kept for12 h at its maximum value and then being dropped and kept at its minimum for a further 12 h. These results were compared against the results obtained in the simulation described in Section 4.2 (where the temperature amplitude was 15°C). This was done in order to test the effect of the amplitude of temperature oscillation on absolute humidity and solids moisture content. As seen in Figures 7*a*–7*c*, where results at a penetration depth of 0.005 m from the bag–environment boundary (the sugar–bag interface) are presented, increasing temperature amplitude caused the amplitudes of absolute humidity and solids moisture content to increase accordingly. This result was anticipated, since higher amplitudes of the temperature square wave would cause sharper gradients. As before, the solids moisture content at a depth of 0.005 m from the external boundary was seen to decrease. As expected, the decrease was sharper for higher temperature amplitudes, because of the sharper changes in the equilibrium humidity of the system in this region.

4.4. The Effect of the Oscillating Temperature Average on Heat and Mass Transfer

In order to study the effect of the oscillating temperature average T_m, simulations were performed with the same initial conditions and the same amplitude of the temperature square wave (15°C) as in the case described in Section 4.2, but with different oscillating temperature averages, namely, 20°C (oscillations between 35°C and 5°C) and 30°C (oscillations between 45°C and 15°C). As before, ten 24-h cycles were simulated. Figure 8 presents the variations in temperature, absolute humidity, and solids moisture content profiles at two penetration depths of 0.005 (sugar–bag interface) m and 0.6 m (bag core) from the external boundary.

In Figure 8*a*, the temperatures at 0.005-m depth could be seen to respond quickly to the external fluctuations and were observed to behave in a sawtooth manner. Since the boundary temperature wave amplitudes were the same, the temperature profiles would overlap if shifted upward with increasing oscillating temperature average. In the bag core (Figure 8*b*), the temperatures were seen to follow the behavior described in Section 4.2 for the central regions, with their values tending to the oscillating temperature average value.

Figures 9*a* and 9*b* show the variation in the profiles of absolute humidity at penetration depths of 0.005 m and 0.6 m, respectively. At 0.005-m depth the absolute humidity was seen to oscillate, following the temperature behavior. The peak of these oscillations increased with increasing T_m. This was due to the fact that when the maximum temperature was higher (for higher T_m), the equilibrium relative humidity decreased to a lower value (for a discussion of the equilibrium behavior of hygroscopic materials, see [21]), hence more liquid would need to evaporate from the sugar grain surface to replenish the vapor content of the air in order for the system to reach equilibrium again. Moreover, it could be seen that the trough of the absolute

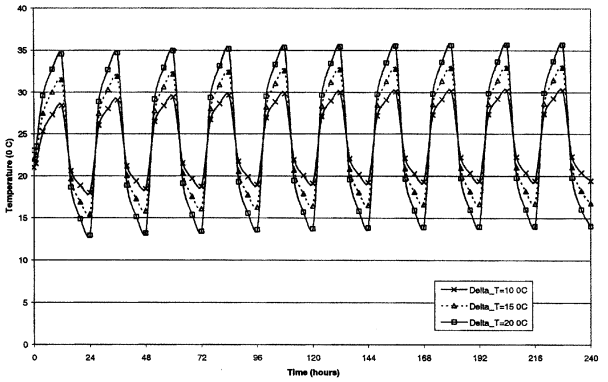

(a)

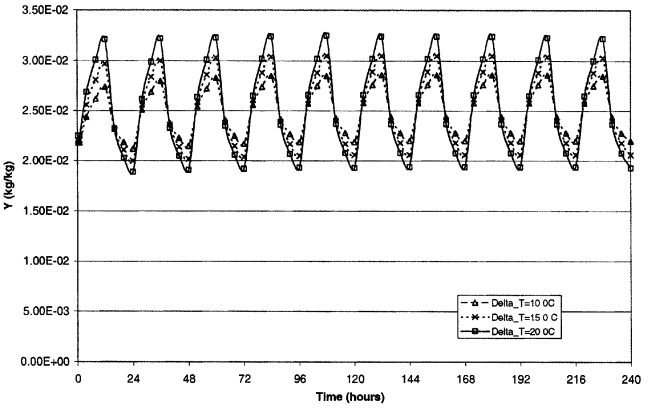

(b)

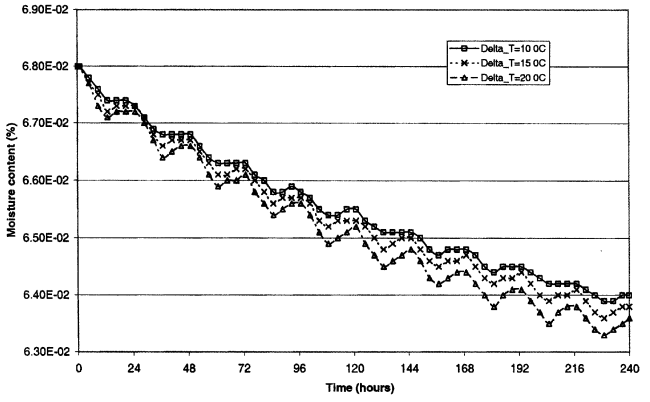

(c)

Figure 7. Impact of different temperature oscillation amplitudes on sugar at a penetration depth of 0.005 m from the external boundary: (*a*) temperature, (*b*) absolute humidity, and (*c*) solids moisture content.

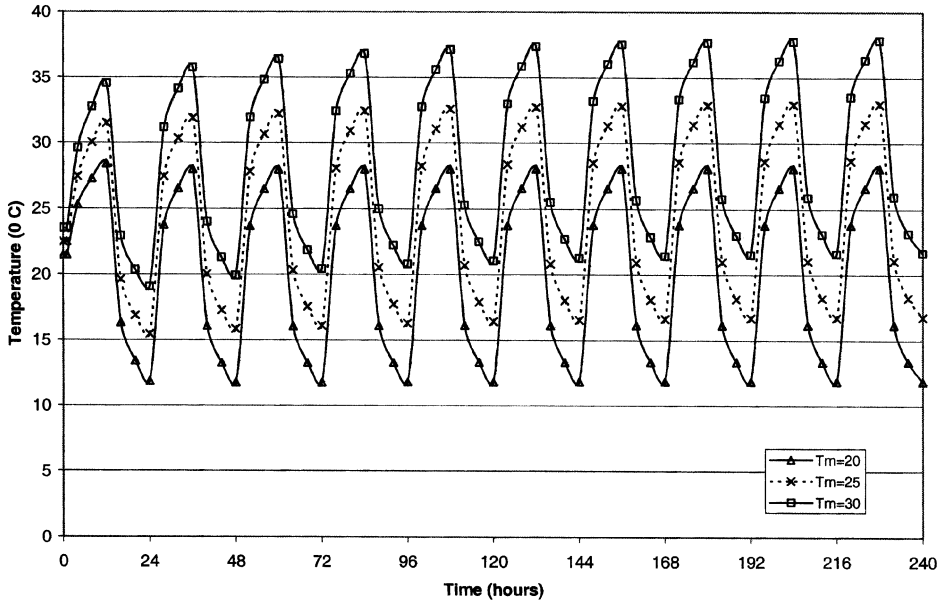

(a)

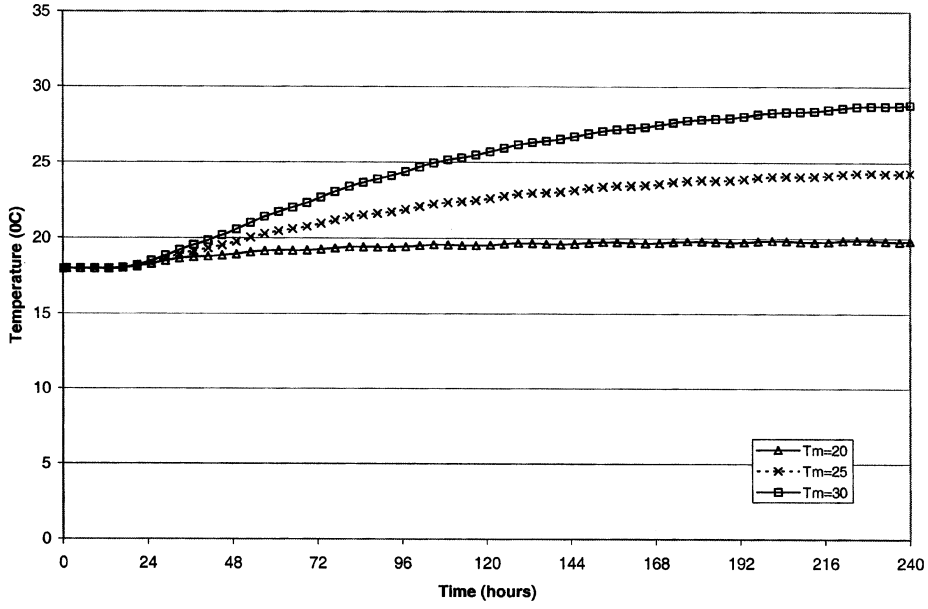

(b)

Figure 8. Impact of different oscillating temperature averages on temperature variation at penetration depths of (*a*) 0.005 m and (*b*) 0.6 m from the external boundary.

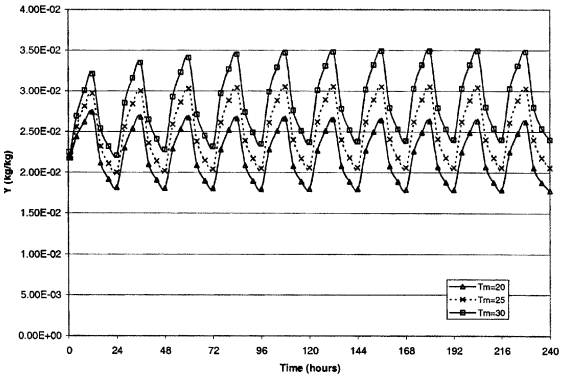

(a)

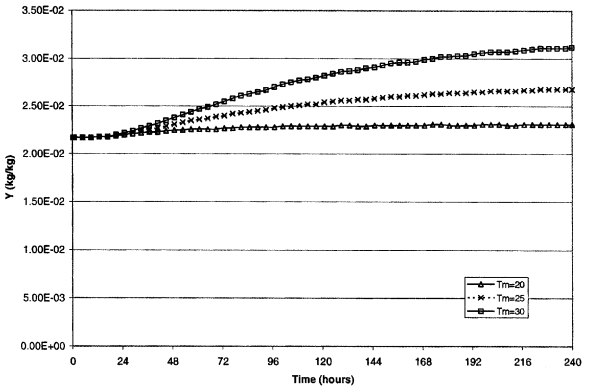

(b)

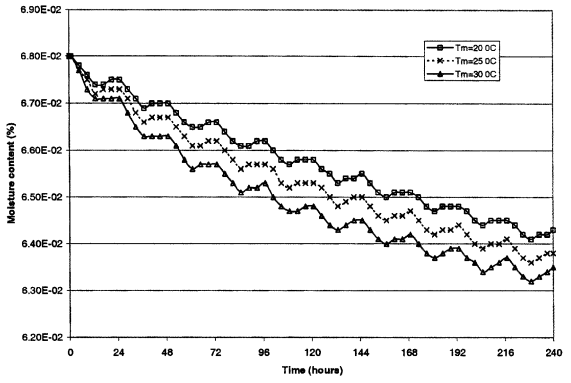

(c)

Figure 9. Impact of different oscillating temperature averages on absolute humidity [at penetration depths of (*a*) 0.005 m and (*b*) 0.6 m from the external boundary] and solids moisture content profiles [at penetration depth of (*c*) 0.005 m from the external boundary].

humidity oscillations decreased with decreasing T_m. This again could be explained through the lower minimum temperature (for lower T_m), which would cause the equilibrium relative humidity to increase more, hence requiring condensation of more vapor from the air onto the solid to drive the system back into equilibrium. Hence, the system would be depleted of vapor faster and the absolute humidity would be expected to be lower. At the bag core (Figure 9*b*), absolute humidity was seen to exhibit a pattern similar to that of the temperature (with the equilibrium value increasing with increasing T_m).

Figure 9*c* presents the changes in the profiles of the solids moisture content at a penetration depth of 0.005 m from the external boundary. It could be seen that the moisture content exhibited an oscillating behavior (as indeed was the case for temperature and absolute humidity). The decreasing trend was anticipated and the sharpest decrease occurred for the highest T_m, since for that T_m, the absolute humidity increase in the bag core was the highest.

5. CONCLUDING REMARKS

In this article, a dynamic model of coupled heat and mass transfer with phase change and absorption/desorption in porous media has been presented. The transient heat and moisture transfer of granulated sugar within a big bag have been simulated using the finite-volume method for oscillating ambient environmental conditions. Predicted temperature and moisture content profiles were compared with available experimental data and very good agreement was established. It was found that the temperature close to the bag–environment boundary region responded very quickly to changes of the boundary temperature. The temperature in the core of the bag approached the oscillating temperature average with time. The evaporation and condensation of moisture occurred due to temperature change. The moisture content close to the bag–material interface responded more quickly to changes in environmental temperature than the moisture content at the bag core. It was found that the intensity of the moisture absorption and desorption processes was highest within a penetration depth of 0.2 m from the external boundary. As was discussed, the moisture content close to the bag–material interface decreased in order to replenish the vapor content of the air in the bag core regions, which increased as a result of the slow increase in temperature in these regions. It was shown that moisture migration in big bags can be reduced by decreasing the oscillating temperature amplitudes and the oscillating temperature average, and also by increasing the bag thickness or changing the bag material to a less heat-conducting one. It is believed that the model can be employed not only to predict moisture migration but may also be used in other scientific and engineering fields involving heat and mass transfer in porous media, where convection and radiation are not significant.

REFERENCES

1. K. Rastikian and R. Capart, Mathematical Model of Sugar Dehydration during Storage in a Laboratory Silo, *J. Food Eng.*, vol. 35, pp. 419–431, 1998.
2. M. S. A. Bradley, R. J. Farnish, A. N. Pittman, and M. C. Leaper, Caking by Moisture Migration—An Investigation of Causes, *Trans. Inst. Mech. Eng.*, vol. 3, pp. 39–46, 2000.

3. O. Mikus and L. Budicek, Sugar Storage in Silos, *Sugar Technol. Rev.*, vol. 13, pp. 53–129, 1986.
4. T. P. Labuza and C. R. Hyman, Moisture Migration and Control in Multi-domain Foods, *Trends Food Sci. Technol.*, vol. 9, no. 2, pp. 47–55, 1998.
5. J. R. Phillip and D. A. DeVries, Moisture Movement in Porous Materials under Temperature Gradients, *Trans. Am. Geophys. Union*, vol. 38, no. 2, pp. 222–232, 1957.
6. A. Bouddour, J.-L. Auriault, M. Mhamdi-Alaoui, and J.-F. Bloch, Heat and Mass Transfer in Wet Porous Media in Presence of Evaporation-Condensation, *Int. J. Heat Mass Transfer*, vol. 41, no. 15, pp. 2263–2277, 1998.
7. A. Holstad, Temperature-Driven Fluid Flow in Porous Media Using a Mixed Finite Element Method and a Finite Volume Method, *Adv. Water Resources*, vol. 24, no. 8, pp. 843–862, 2001.
8. Y. Le Bray and M. Prat, Three-Dimensional Pore Network Simulation of Drying in Capillary Porous Media, *Int. J. Heat Mass Transfer*, vol. 42, no. 22, pp. 4207–4224, 1999.
9. P. Perré and I. W. Turner, A 3-D Version of TransPore: A Comprehensive Heat and Mass Transfer Computational Model for Simulating the Drying of Porous Media, *Int. J. Heat Mass Transfer*, vol. 42, pp. 4501–4521, 1999.
10. M. Prat, Recent Advances in Pore-Scale Models for Drying of Porous Media, *Chem. Eng. J.*, vol. 86, no. 1–2, pp. 153–164, 2002.
11. L. M. Bryntesson, Pore Network Modelling of the Behaviour of a Solute in Chromatography Media: Transient and Steady-State Diffusion Properties, *J. Chromatogr. A*, vol. 945, no. 1–2, pp. 103–115, 2002.
12. J. Fan, Z. Luo, and Y. Li, Heat and Moisture Transfer with Sorption and Condensation in Porous Clothing Assemblies and Numerical Simulation, *Int. J. Heat Mass Transfer*, vol. 43, no. 16, pp. 2989–3000, 2000.
13. J. Crank, *The Mathematics of Diffusion*, 2nd ed., Oxford University Press, Oxford, UK, 1975.
14. D. A. DeVries, Simultaneous Transfer of Heat and Moisture in Porous Media, *Trans. Am. Geophys. Union*, vol. 39, pp. 909–916, 1958.
15. A. V. Luikov, *Heat and Mass Transfer in Capillary-Porous Bodies*, Pergamon, Oxford, UK, 1966.
16. R. Ranjan, J. Irudayaraj, and J. Mahaffy, Modelling Simultaneous Heat and Mass Transfer Using the Control-Volume Method, *Numer. Heat Transfer B*, vol. 41, pp. 463–476, 2002.
17. L. S. Oliveira and K. Haghighi, Conjugate Heat and Mass Transfer in Convective Drying of Porous Media, *Numer. Heat Transfer A*, vol. 34, pp. 105–117, 1998.
18. J. Irudayaraj, Y. Wu, A. Ghazanfari, and W. Yang, Application of Simultaneous Heat, Mass, and Pressure Transfer Equations to Timber Drying, *Numer. Heat Transfer A*, vol. 30, pp. 233–247, 1996.
19. M. C. Leaper, M. S. A. Bradley, J. A. S. Clearver, I. Bridle, A. R. Reed, H. Abou-Chakra, and U. Tüzün, Constructing an Engineering Model for Moisture Migration in Bulk Solids as a Prelude to Predicting Moisture Migration Caking, *Adv. Powder Technol.*, vol. 13, pp. 411, 2002.
20. C. H. A. Molenda, P. Crausse, and D. Lemarchand, Heat and Humidity Transfer in Non Saturated Porous Media: Capillary Hysteresis Effects under Cyclic Thermal Conditions, *Int. J. Heat Mass Transfer*, vol. 36, no. 12, pp. 3077–3088, 1993.
21. N. Christakis, Modelling of the Microphysical Processes That Lead to Warm Rain Formation, Ph.D. thesis, UMIST, Manchester, UK, 1998.
22. J. R. Rogers and M. K. Yau, *A Short Course on Cloud Physics*, Pergamon Press, London, UK, 1989.

23. J. E. Warren and P. J. Root, The Behaviour of Naturally Fractured Reservoirs, *Soc. Petrol. Eng. J.*, vol. 3, pp. 245–255, 1963.
24. R. W. Zimmerman, T. Hadgu, and G. S. Bodvarsson, A New Lumped-Parameter Model for Flow in Unsaturated Dual-Porosity Media, *Adv. Water Resources*, vol. 19, no. 5, pp. 317–327, 1996.
25. H. K. Versteeg and W. Malalasekera, *An Introduction to Computational Fluid Dynamics: The Finite Volume Method*, Prentice Hall, 1996.
26. M. Cross, Computational Issues in the Modelling of Materials Based Manufacturing Processes, *J. Comput. Aided Mater. Design*, vol. 3, pp. 100–116, 1996.
27. *PHYSICA Theory Manual*, The University of Greenwich, 2001, www.greenwich.ac.uk/~physica.
28. M. C. Leaper, M. S. A. Bradley, K. Sinclair, A. Barnes, and E. Dean, Investigating Temperature Fluctuation, Moisture Migration and Cake Formation in Big-Bags Using Heat Transfer Modelling and Intermediate Scale Caking Rig, QPM Case Study Report, University of Greenwich, London, UK, March 2001.